



國立臺灣大學醫學院暨工學院醫學工程學系

碩士論文

Department of Biomedical Engineering

College of Medicine and College of Engineering

National Taiwan University

Master thesis

波浪狀纖維結構促進早衰素表現血管平滑肌細胞收縮型

Wavy Fiber Structure Improves Contractile Phenotype of  
Progerin-expressing Vascular Smooth Muscle Cells

林俊宇

Chun-Yu Lin

指導教授：趙本秀博士

Advisor: Pen-Hsiu Grace Chao, Ph.D.

中華民國 111 年 3 月

March, 2022

國立臺灣大學碩士學位論文  
口試委員會審定書



波浪狀纖維結構促進早衰素表現血管平滑肌細胞收縮型  
Wavy Fiber Structure Improves Contractile Phenotype of  
Progerin-expressing Vascular Smooth Muscle Cells

本論文係 林俊宇 君 (學號 R07528037) 在國立臺灣大學醫學工程學系完成之碩士學位論文，於民國 111 年 3 月 22 日承下列考試委員審查通過及口試及格，特此證明

口試委員：

趙本杰

紀毓惠 (指導教授) 李本龍

系主任：

王東志

## 致謝



在碩士班的過程，所幸有身旁貴人們的陪伴讓我成長不少，對好奇事物的探索，不管是提問或是假設的求證，變為更加務實且耐心地實事求是，同時培養邏輯思考並成為能解決問題的人。每當因實驗細節感到困惑，感謝趙本秀老師適時提供指引，助我梳理頭緒以克服難題。感謝紀雅惠老師、郭柏齡老師擔任我預口試及口試的委員，提供許多建設性的指導以改善我論文的不足。感謝台大貴儀共軛焦顯微鏡技術員莊小姐、吳小姐耐心教導顯微鏡的使用。感謝國衛院生藥所王靖雅助理不辭辛勞安排實驗鼠源。感謝醫工所李素秋小姐熱心、有效率幫忙我處理許多文件。感謝黃書彥學長、黃勁勛學長、溫文慈學姊、張峻瑋學長、廖文寧學姊、可愛的黃柏霖學長用心傳授經驗、分享研究看法。感念實驗室夥伴們與我朝夕相處的時光，讓我反思實驗設計的不足。感謝我的父母，無時無刻的關懷與堅定的支持。回想碩士班的日子，儘管遭遇數不清的瓶頸與挫折，慶幸有你們的陪伴與幫忙，讓我總能迎刃而解，承載大家給予的祝福，我將邁入人生的下一個階段，持續面對新的挑戰。

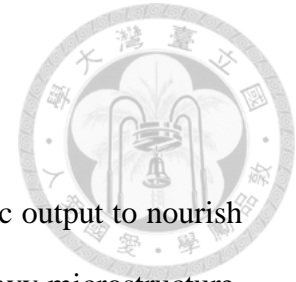
## 中文摘要



彈性動脈緩衝來自心搏的血壓波動以穩定提供器官血液，此彈性機械性質來自血管壁間質之環繞波浪狀微結構，而老化或受傷的動脈因彈性組織纖維結構與成分的改變導致硬度上升與功能受損。血管平滑肌細胞維持動脈結構與功能恆定，在成長、修復或疾病過程中，血管平滑肌細胞可從收縮型轉變為合成型以促進細胞增殖與胞外基質分泌，此表現型調控若失衡可能誘發血管修復不良與血管疾病惡化；目前雖有不少研究探討環境化學因子對血管平滑肌表現型的調控，不過組織纖維結構本身對血管平滑肌的影響卻尚未釐清。本研究以電紡絲技術製造仿生纖維，模擬健康動脈的捲曲或是老化受傷動脈的直線結構，以期釐清結構型態對細胞的調控。此外，在疾病動物模式發現表現早衰素的血管平滑肌細胞會加速血管的病變，因此我們也研究早衰素對血管平滑肌表現型的影響，並綜合性探討組織纖維排列與早衰素對血管平滑肌的調控。研究結果發現，捲曲纖維結構雖對正常血管平滑肌的效應微弱，但對帶有早衰素的血管平滑肌細胞則效果顯著。捲曲纖維結構除可緩衝血壓波動，本研究也指出其對血管平滑肌表現型調節的重要性；同時，探索血管恆定的調控對了解血管疾病機轉高度重要，而我們的仿生纖維平台適用於發展血管疾病的模擬並有助於新藥的開發。

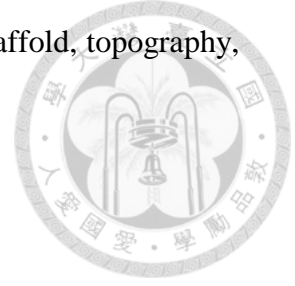
關鍵字:微結構、動脈、血管平滑肌表現型多元性、仿生纖維平台、早衰素

## Abstract



Elastic arteries smoothen the pulsatile blood flow from cardiac output to nourish the organs. Elastic fibers in arterial wall form circumferentially wavy microstructure, contributing to the mechanical functionality. In aged or injured arteries, elastic fibers undergo morphological and compositional changes, resulting in arterial stiffening and loss of tissue function. In the arterial wall, contractile vascular smooth muscle cells (VSMCs) maintain the mechanical functionality of the tissue. During vessel growth, repair, or pathogenesis, VSMCs become proliferative and synthesize abundant matrix components, known as the synthetic phenotype. Imbalanced VSMC plasticity induces adverse arterial remodeling and progression of vascular diseases. Environmental cues regulate phenotypic flexibility of VSMC, but the roles of matrix organization remain largely unknown. To address the influence of fiber structure on VSMC phenotype, we established VSMC culture in straight or wavy scaffold, which structurally mimics the aged/injured or healthy arteries. Additionally, we used progerin-expressing VSMCs, which drive vascular alternation in disease model animals, to investigate progerin and topography interaction. We found that while wavy topography slightly promoted contractile phenotype of wild-type (WT) VSMC, the effect was more robust in progerin-expressing VSMC. Our study indicated that wavy fiber structure played significant roles in regulating VSMC phenotype besides its mechanical contribution. Identifying regulatory factors involved in arterial homeostasis will help uncover mechanism of vascular pathology, and our biomimetic scaffold offers a relevant platform for disease modeling as well as new drug discovery.

Keywords: microstructure, artery, VSMC plasticity, biomimetic scaffold, topography, progerin



# Contents



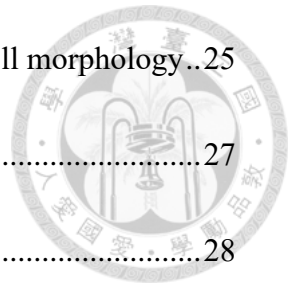
致謝.....	I
中文摘要.....	II
Abstract.....	III
Contents .....	V
List of Figures.....	VIII
Chapter 1 Introduction.....	1
1.1 Arterial structure and function .....	1
1.1.1 Tunica Intima .....	1
1.1.2 Tunica Adventitia .....	1
1.1.3 Tunica Media .....	2
1.2 Vascular aging.....	3
1.1.4 Endothelial dysfunction .....	3
1.1.5 Arterial stiffening .....	4
1.3 Pathogenic roles of VSMC plasticity.....	5
1.4 Molecular mechanism of VSMC phenotype regulation .....	6
1.5 Microenvironmental regulation of VSMC phenotype .....	7
1.6 Accelerated vascular aging model: Hutchinson-Gilford progeria syndrome .....	8

1.7	Vascular tissue engineering.....	10
1.8	Aims of study.....	11
<b>Chapter 2 Material and methods.....</b>		<b>12</b>
2.1	Fabrication of electrospun scaffold.....	12
2.2	Mechanical and structure characterization.....	12
2.3	Scaffold sterilization and coating.....	13
2.4	Mouse aortic vascular smooth muscle cells (VSMCs) isolation and explant culture .....	13
2.5	Cell culture.....	14
2.6	AlamarBlue assay .....	15
2.7	Immunofluorescence staining .....	16
2.8	Microscopy .....	16
2.9	Fluorescent image analysis .....	17
2.10	RNA extraction .....	18
2.11	cDNA synthesis and Quantitative Polymerase Chain Reaction (qPCR) .	18
2.12	Western blot .....	19
2.13	Statistics .....	20
<b>Chapter 3 Results.....</b>		<b>23</b>
3.1	Establish primary VSMC culture and phenotype characterization .....	23





3.2	Characterization of biomimetic fibrous scaffolds and cell morphology..	25
3.3	Phenotypic assessment: VSMC Proliferation .....	27
3.4	Phenotypic assessment: Gene expression profile .....	28
3.5	Phenotypic assessment: Immuno-characterization .....	29
3.6	Progerin induction in VSMCs.....	31
3.7	Phenotypic characterization of progerin-positive cells.....	33
3.8	Effect of progerin expression on VSMC proliferation in scaffold cultures .....	35
3.9	Effect of progerin expression on VSMC gene and protein expression in scaffold cultures .....	36
<b>Chapter 4 Discussion .....</b>		<b>39</b>
<b>References.....</b>		<b>44</b>



# List of Figures



Figure 1. Primary VSMCs exhibit passage-dependent dedifferentiation in 2D cultures. ....24

Figure 2. Electrospun straight (S) and crimp (C) fibrous scaffolds and VSMC morphology in the scaffolds. ....26

Figure 3. Real-time monitoring of WT VSMC proliferation in fibrous scaffold. ...27

Figure 4. Topography-dependent phenotype regulation of WT VSMC at transcript level. ....28

Figure 5. Immunochemical analysis of topographical influence on VSMC phenotype. ....30

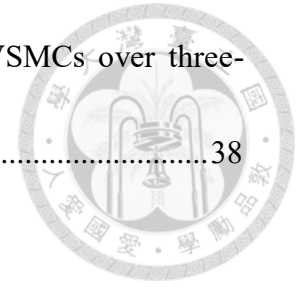
Figure 6. In vitro treatment of 4-OHT induced progerin expression in primary VSMCs. ....32

Figure 7. Phenotypic characterization of progerin-positive VSMCs in 2D cultures. ....34

Figure 8. Real-time proliferation monitoring of progerin-expressing VSMCs in scaffold cultures.....35

Figure 9. Gene profiles of progerin-expressing VSMCs over three-week scaffold cultures. ....37

Figure 10. Immunochemical analysis of progerin-expressing VSMCs over three-week scaffold cultures. .... 38



## List of Tables

Table 1. list of primary and secondary antibodies .....	21
Table 2. list of PCR primers .....	21

# Chapter 1 Introduction



## 1.1 Arterial structure and function

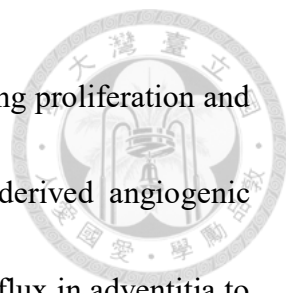
Arterial wall is divided into three layers, tunica intima, tunica media, and tunica adventitia, with different cell types and composition.

### 1.1.1 Tunica Intima

The inner-most structure, tunica intima, is composed of luminal endothelial cells (ECs) and the subendothelial matrix [1]. Luminal lining of ECs forms a hemocompatible surface to sustain blood flow homeostasis [2, 3]. In response to hemodynamic changes, endothelium as an endocrine organ actively regulates vascular tone by releasing factors like nitric oxide (NO) and endothelin, which affect VSMC relaxation and contraction [2, 4]. ECs are also involved in regulation of coagulation and immune response during vascular injury [2, 5, 6].

### 1.1.2 Tunica Adventitia

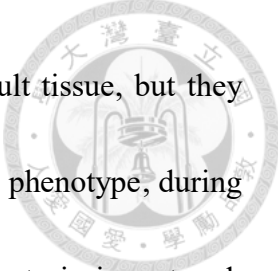
The outermost layer, tunica adventitia, mainly consists of fibroblasts and perivascular nerves embedded in a collagen-rich matrix [7]. Adventitia with heterogeneous cell population and the distinct circulation network, vasa vasorum, contributes to the “outside-in” modulation of arterial remodeling [8]. For example, stress-induced activation of adventitial fibroblasts (AFs) affects phenotypes of neighboring cells and mediates



immune responses. Activated AFs elicit paracrine factors in promoting proliferation and migration of VSMC for neointima formation [9]. Moreover, AF-derived angiogenic factors promote vasa vasorum expansion, facilitating immune cell influx in adventitia to exacerbate vasculopathies [8, 10, 11]. Collectively, the diverse composition of adventitia allows it to be an “injury-responding center” during the arterial remodeling processes [8].

### **1.1.3 Tunica Media**

Centrally located arterial media, composed of multiple lamellar units, serves as the major load-bearing structure of the artery [12]. Circumferentially oriented elastin and collagen envelop resident smooth muscle cells to form functional lamellar units [13]. The passive mechanics of large, elastic arteries are mainly dependent on the amount and organization of elastic fibers in the wall [14]. Layers of concentric lamellae display increased waviness gradient toward the inner wall for uniform stress distribution when subjected to intraluminal distension [15]. The distinct wavy microstructure and matrix constituents of medial lamellae impart the strain-stiffening behavior of the artery [14, 16-18]. The nonlinear property is a protective strategy against arterial overstretch [14, 19]. Medial VSMCs not only control vasomotion but also maintain matrix integrity to ensure the mechanical functionality of arteries. Phenotypic flexibility of VSMC confers it different functional roles in physiologic as well as pathologic arterial remodeling. VSMCs

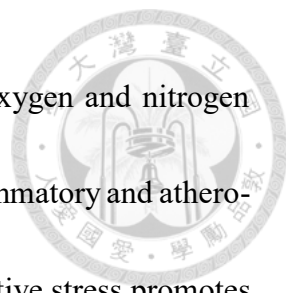


are typically in a quiescent and contractile phenotype in healthy adult tissue, but they become proliferative, migratory, and biosynthetic, known as synthetic phenotype, during embryonic angiogenesis and vessel repair [20]. Once tissue homeostasis is restored, VSMCs regain the contractile phenotype [21]. Although efforts have been made to reveal the underlying mechanisms for VSMC phenotype regulation [22], how pathological changes in the physical environment direct the phenotypic switch of VSMC remains to be elucidated.

## **1.2 Vascular aging**

### **1.1.4 Endothelial dysfunction**

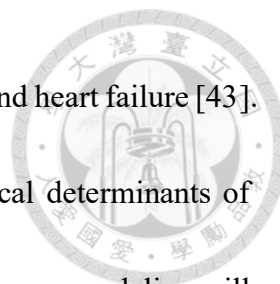
Cardiovascular diseases (CVDs) are the leading cause of death around the world, and aging presents a major risk factor to CVDs [23, 24]. Vascular aging is characterized by impaired structural and functional integrity and has deleterious impact on blood supply for proper organ functions [25]. Excess oxidative stress and chronic low-grade inflammation are major mechanisms of vascular aging, giving rise to endothelial dysfunction and structure alternations [26]. Nitric oxide (NO) plays crucial roles for proper endothelial function including smooth muscle relaxation, inhibition of the attachment of inflammatory cells to endothelium, and down-regulation of the



inflammatory cytokines release [27]. On the other hand, reactive oxygen and nitrogen species (RONS) reduce the NO availability to attenuate the anti-inflammatory and athero-protective effects of NO [28]. Study also suggests that chronic oxidative stress promotes senescence-associated secretory phenotype (SASP) of endothelial cells [29]. The interplays between oxidative stress and inflammation, which not only impair endothelial functions but also induce phenotypic change of endothelial cells, result in further arterial remodeling by VSMCs [26].

### **1.1.5 Arterial stiffening**

Another hallmark of vascular aging is arterial stiffening [30]. Elastic arteries normally smoothen the pulsatile waves generated from cardiac ejection to deliver steady blood flow [31, 32]. With age, elastic arteries become stiffer due to the morphological and compositional alternations of the major structural proteins, elastin and collagen [33]. Elastin fibers, susceptible to mechanical damage and proteolysis, degenerate and reduce the arterial compliance [14, 31, 34]. Meanwhile, generation of elastin-derived peptides (EDPs) from degradation triggers adverse arterial remodeling and osteogenic differentiation of VSMCs to exacerbate elastin degradation and arterial calcification [35, 36]. Furthermore, compensatory collagen deposition reconstitutes the matrix and contributes to the arterial stiffening [31, 37]. Arterial stiffening and its hemodynamic




consequences induce systolic hypertension, coronary artery disease, and heart failure [43]. Homeostasis of matrix integrity and VSMC plasticity are two critical determinants of arterial stiffening [38]. Identifying aging factors that foster adverse artery remodeling will provide useful insights into improving cardiovascular health.

### **1.3 Pathogenic roles of VSMC plasticity**

The different functions that VSMC can perform translate into phenotypic flexibility, ranging from contractile to synthetic [22]. VSMC plasticity is involved in a myriad of vascular adaptations from early vascular development to vascular repair and pathogenesis. Early vascular aging can be thought of as an inadequate arterial repair to various mechanical, metabolic and chemical stresses [39]. Age-associated pro-inflammatory signaling promotes phenotypic change of VSMC and progressive intimal thickening [40, 41]. Matrix remodeling in turn stimulates calcification of VSMC, accelerating arterial stiffening [42]. VSMC phenotypic transition also facilitates development of atherosclerosis by synthesizing athero-prone matrix and cytokine production for inflammation propagation [43]. Proteoglycans (PGs) produced by synthetic VSMCs promote intimal retention of lipoproteins, which initiates further VSMC proliferation and synthesis of lipoprotein-attracting PG, driving atherosclerotic lesion formation [44]. In



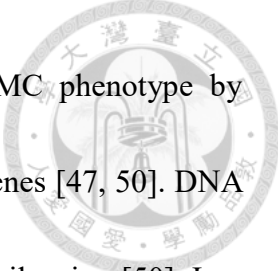


advanced atherosclerosis, most atheroma foam cells, characterized by impaired cholesterol efflux function, originate from VSMC rather than macrophage [45]. Given diverging roles of VSMC in a broad range of CVDs, targeting mechanism of VSMC phenotype regulation is crucial to develop strategies against CVDs [46].

#### **1.4 Molecular mechanism of VSMC phenotype regulation**

Adult VSMCs are generally in the differentiated contractile phenotype, but growth factors or inflammatory cytokines silence the expression of contractile genes and potentiate their ability to proliferate, migrate, and synthesize matrix proteins [47].

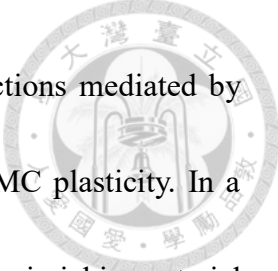
Transcription and epigenetic modifications are critical mechanisms shaping the plasticity program [21]. At the transcript level, a 10-base pair CArG-box sequence within the promoter is conserved among several VSMC contractile markers including  $\alpha$ -SMA ( gene *ACTA2*), SM22 ( gene *TAGLN*), Calponin-1 (gene *CNN1*), and myosin heavy chain 11 (gene *MYH11*) [21]. Association of the CArG element with its regulator serum response factor (SRF) and coactivator myocardin (MYOCD) forms a transcriptional complex and activates expression of contractile genes for VSMC maturation [21, 48]. On the other hand, potent repressors such as Krüppel-like factor 4 (KLF4) down-regulates expression of contractile genes by inhibiting SRF-MYCOD binding to CArG elements [48, 49]. At



the epigenetic level, chromatin-modifying enzymes modulate VSMC phenotype by controlling the accessibility of transcriptional regulators to marker genes [47, 50]. DNA methylation is a well-studied epigenetic modification linked to gene silencing [50]. In a vessel-injury murine model and human atherosclerotic samples, up-regulated DNA methylation enzyme DNMT3A increases methylation of CArG elements in contractile genes to promote pathogenic transition of VSMCs [51]. In addition, loss of histone H3 lysine 9 di-methylation (H3K9me2) at inflammation-responsive VSMC genes enhances vascular remodeling and progression of CVDs [52]. Of note, key environmental cues affecting VSMC genetic program to modulate the phenotypic transition, remain poorly understood.

### **1.5 Microenvironmental regulation of VSMC phenotype**

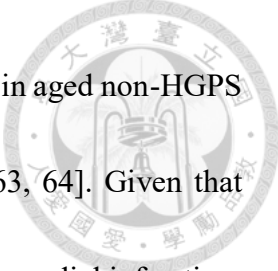
VSMC cultured in vitro exhibits phenotypic transition owing to the lack of environmental cues necessary for phenotype maintenance [53, 54]. ECM with biochemical and biophysical properties forming three-dimensional microenvironment affects cell fate [55]. For example, fibronectin promotes the synthetic VSMC phenotype, while laminin promotes the contractile phenotype [56, 57]. Disruption of elastin-VSMC connection interrupts cell–matrix signaling and contributes to VSMC phenotype



transition and arterial occlusion [58]. In addition to regulatory functions mediated by matrix chemistry, biophysical features of the matrix also affect VSMC plasticity. In a hydrogel platform with tunable stiffness, VSMCs on the stiffer gel mimicking arterial stiffening display synthetic phenotype with enhanced response to growth factor [59, 60]. In micro-pattern studies, topography regulates VSMC elongation and alignment, and promotes the contractile phenotype [54, 61]. Medial lamellae forming three-dimensional wavy microstructure confer critical mechanical functionality [15, 16]. Besides the mechanical contribution, the biological role of lamellar waves in VSMC phenotype regulation remains to be investigated.

## **1.6 Accelerated vascular aging model: Hutchinson-Gilford progeria syndrome**

Hutchinson-Gilford progeria syndrome (HGPS) is a rare and fatal premature aging syndrome caused by the accumulation of a mutant *LMNA* gene product, progerin [62]. Lamin A/C, the normal protein products of *LMNA* gene, are nucleoskeleton proteins that are involved in a broad range of cellular functions, including nuclear mechanical stability and chromatin organization [63]. Aberrant progerin production leads to irregular nuclear morphology and gene dysregulation. HGPS patients manifest premature aging features, such as alopecia, muscular weakness, and osteoporosis, and die of occlusive vascular



diseases at puberty [63]. Notably, low level of progerin is also present in aged non-HGPS individuals, suggesting HGPS as a model for physiological aging [63, 64]. Given that major causes of death in HGPS population are atherosclerosis and myocardial infarction, issue about how progerin leads to CVDs in HGPS model remains to be addressed. Arteries of HGPS patients have progressive loss of medial VSMCs and prominent fibrosis and calcification of arterial wall [62]. Although progerin expression was found in all vascular cells [62], VSMC-specific progerin expression in a mouse model is sufficient to accelerate atherosclerosis [65, 66]. Progerin-associated structural and functional alternations in nuclear lamina underlie the mechanisms of HGPS pathology. In structural theory, progerin reduces lamin A dynamics and impairs nuclear mechanosensitivity, rendering cells more susceptible to physical stimuli [67, 68]. In gene regulation theory, progerin disrupts lamin A/C-chromatin interactions and alters epigenetic modifications, leading to genome instability [68, 69]. Mechanotransduction bridges structure and gene regulation theories, suggesting that change in either nuclear mechanoresponsive structures or genetic outputs impairs mechanotransduction signaling and results in disease phenotypes [70].



## 1.7 Vascular tissue engineering

Tissue engineering uses componential and structural imitation to facilitate tissue regeneration [71]. In the design of tissue-engineered blood vessels (TEBV), biomechanically competent construct is an important element [72]. In vascular constructs, diverse fabrication approaches, including 3D printing, electrospinning, and sheet rolling, are based on tissue structure mimicry [72]. Establishment of physiologically relevant environment provides a better tissue model for clinical application as well as disease modeling. Electrospun scaffolds, composed of easily tunable compositions and structures, closely mimic fibrous tissues [71, 73]. Studies had examined influence of matrix physical properties on VSMC phenotype by manipulation of fiber diameter and stiffness of the electrospun scaffolds [74, 75]. Taken advantage the versatility of electrospun scaffolds, we investigate the effects of fiber topography on VSMC plasticity. Straight scaffolds recapitulated the fiber structure of aged/injured arteries, and wavy fibrous scaffolds, obtained from post-processing of straight materials, resembled the non-linear behavior and fiber organization of the physiologically healthy arteries. To better represent vascular aging model, we also incorporated progerin-expressing VSMC into these scaffolds to study the interactive effects of progerin and topography.



## 1.8 Aims of study

Given that phenotype transition or even loss of medial VSMC is accompanied by altered matrix morphology, we focused on the instructive roles of matrix architecture on VSMC phenotype. We hypothesized that wavy fiber structure promoted the re-differentiate of VSMC. To test the hypothesis, we established primary culture of murine VSMC and characterized VSMC de-differentiation in 2D culture. Next, we produced straight or crimp scaffold, which structurally and mechanically recapitulated aged/injured or healthy arteries, as the 3D culture construct, and characterized topographical regulation of VSMC phenotype.

In addition to topographical manipulation, we established inducible progerin-expressing VSMC culture. We quantified progerin expression level with passaging and characterized progerin influence on VSMC phenotype in 2D culture. Finally, we investigated combined effects of progerin and topography on regulation VSMC by phenotypic characterization of progerin-expressing VSMCs cultured in biomimetic scaffolds.

## Chapter 2 Material and methods



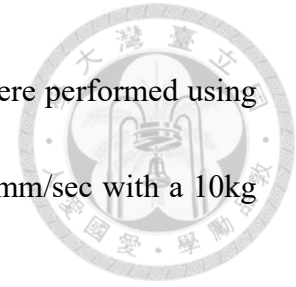
### 2.1 Fabrication of electrospun scaffold

Poly-L-lactide solution (PLLA, 6% w/v in hexafluoropropylene) was spun at a flow rate of 3 ml/hr with an applied voltage of 8kv and gap distance of 13cm. Polyethylene oxide solution (PEO, 13%w/v in 80% ethanol) was spun at flow rate 0.9ml/hr with an applied voltage 8kv and gap distance of 13.5cm. The collector voltage and shield voltage were -4kv and 3kv, respectively. Two polymeric materials were extruded simultaneously from two nozzles placed on opposite sides and collected on a rotating mandrel (1200rpm) to form aligned composite PLLA/PEO scaffold at the weight ratio 7:3. For the preparation of straight scaffolds, composite scaffolds were rinsed in deionized water for an hour to remove sacrificial PEO fibers and sandwiched between two glass slides for a 15 min-heating at 48°C on the hot plate. For wavy scaffolds, composite scaffolds were rinsed in 75% ethanol followed by 30 mins of wash in deionized water. Subsequently, scaffolds were also sandwiched and heated on the hot plate at 85°C for 15 mins.

### 2.2 Mechanical and structure characterization

The thickness of each scaffold (1x4 cm<sup>2</sup>) was measured using a laser optical sensor (Micro-Epsilon ILD 1420). Ten different regions of each scaffold were detected to

estimate the average scaffold thickness. The uniaxial tensile tests were performed using the test instrument (BOSE ElectroForce 5500) at a strain rate 0.02 mm/sec with a 10kg load cell.



To quantify fiber structure, air dried scaffolds were imaged at 1000x using a scanning electron microscope (SEM, Hitachi TM3000). The SEM images were analyzed with the Neuron J plugin in Fiji to measure fiber crimpness by tracing the fiber trajectory. Fiber crimpness was defined as 1- (end-to-end distance of a fiber / contour length).

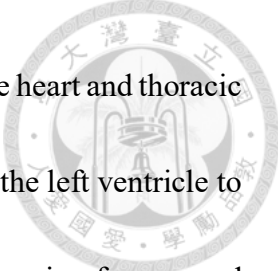
### **2.3 Scaffold sterilization and coating**

Large sheets of electrospun mats were cut into small scaffolds (1x2 cm<sup>2</sup>) with long axis parallel to fiber orientation. For sterilization, scaffolds were soaked in 75% ethanol for 1 min followed by immersion in 35% hydrogen peroxide for an hour. For scaffold coating, scaffolds were pre-coated with dopamine hydrochloride (2mg/ml, ph 8.5) for 15 min. After that, scaffolds were incubated in type 1 collagen solution (90µg/ml, BD354249) at 37°C overnight.

### **2.4 Mouse aortic vascular smooth muscle cells (VSMCs) isolation and explant culture**

VSMCs were isolated from the thoracic aortas of 8 to 10-week-old mice. Mouse was euthanized with CO<sub>2</sub> and immobilized on a styrofoam board in supine position for dissection. Sterile surgical forceps and scissor were used to open the mouse abdomen and

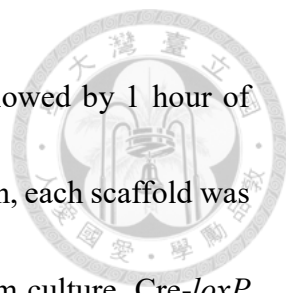




remove the visceral organs. Then, the rib cage was opened to expose the heart and thoracic aorta. Before the thoracic aorta was cut, sterile PBS was injected into the left ventricle to rinse the aorta. Fat and connective tissues on the aorta were removed by microforceps and tweezers. The aortic segment below the aortic arch and above the diaphragm was cut for tissue explant culture. The isolated thoracic aorta segment was transferred to a dish containing sterile PBS for additional cleaning process visualized with dissecting microscope. The clean aorta was cut longitudinally and the intima layer was gently scraped off with a tweezers to eliminate the endothelial cells. In the final step, the aorta segment was cut into small pieces and distributed evenly to four droplets of media dripped on a new 6 cm dish. Four coverslips were placed on each drop to press down the floating aortic pieces. The culture dish was filled with additional 5ml media and was carefully put into the incubator. After two-week-incubation, primary VSMCs growing out from the aortic pieces reached confluence without medium replacement.

## **2.5 Cell culture**

Primary VSMCs harvested from tissue explant culture were seeded at 550 cells/cm<sup>2</sup> on culture dish in DMEM/F-12 (1:1) (Gibco 11330032) supplemented with 10% FBS and 1% GlutaMAX (Gibco 35050061). Cells were passaged when reaching 90% confluency, and cell numbers were tracked to calculate cell doubling time. For cell seeding in



scaffolds, each side received a 70µl aliquot with 7500 P6 cells followed by 1 hour of incubation for the cells to attach. After a two-hour attachment duration, each scaffold was transferred into 12-well plate filled with 1.5ml medium for long-term culture. *Cre-loxP* mouse model with the inducible progerin gene was obtained from Dr. Ya-hui Chi of NHRI. Briefly, a mouse was inserted with a vector containing a *loxP*-flanked PGK-neo-4xpA cassette and human progerin tagged with FLAG at the ROSA26 locus. The cassette can be removed with the expression of Cre recombinase after the treatment of 4-hydroxytamoxifen (ab141943, 4-OHT). P1 VSMCs were cultured for 3 days and then treated with 4-OHT (1:2000 in medium at final concentration: 1µM) for 48hr to induce progerin expression. Afterwards, medium containing 4-OHT was replaced with fresh medium for further incubation.

## 2.6 AlamarBlue assay

Single scaffold (1x2 cm<sup>2</sup>) in each well of 12-well plate was incubated in 1.5ml fresh medium at 37°C overnight. Next day, scaffold cultures were supplemented with AlamarBlue dye (Invitrogen Cat#DAL1100) in an amount equal to 10% of total volume into medium and incubated at 37°C for 3 hrs. After incubation, 100µl of culture medium was aspirated into microplate for fluorescent detection by the plate reader (Synergy HTX, BioTek) at excitation wavelength of 530 nm and emission wavelength of 590 nm. Signal

intensity was normalized to the medium control without cells. Scaffolds were washed in PBS following AlamarBlue incubation and cultured in fresh medium for subsequent experiments.



## 2.7 Immunofluorescence staining

VSMCs were fixed with 37°C 4% formaldehyde (Macron Fine Chemicals) for 10 mins followed by permeabilization with 0.5% (v/v) Triton X-100 (Sigma) for 20 mins. Cells were then blocked with 1% (w/v) BSA (Urinogen) in PBS at 4°C overnight.  $\alpha$ -SMA, SM22, Calponin-1, and Progerin (tagged with FLAG) were stained using corresponding combination of primary antibodies (Table 1) diluted in 1% BSA at room temperature for an hour. Afterwards, cells were incubated with corresponding secondary antibodies (Table 1) diluted in 1% BSA, and were counterstained with DAPI (5 $\mu$ g/ml, Sigma Cat#D8417) and Alexa Fluor 568 phalloidin (1:200 in 1% BSA, Invitrogen Cat#A12380) at room temperature for an hour. Following staining steps, Fluoromount aqueous mounting medium (Sigma Cat#F4680) was used to embed samples between coverslip and slide.

## 2.8 Microscopy

Fluorescent images were acquired with Nikon Eclipse Ti2 E inverted microscope equipped with CCD camera (Hamamatsu) and 20X/NA0.45 air objectives (Nikon). Confocal images were taken by a Leica SP8 confocal microscope with 20X/NA0.75 and

63X/NA1.4 oil immersion objectives.



## 2.9 Fluorescent image analysis

To quantify the expression of VSMC contractile markers and progerin in cell populations, image contrast was controlled by setting lower and upper limits of the display range in Fiji. Cell identity was recognized by nucleus and F-actin signals labeled by DAPI and phalloidin. For determination of minimum values (lower display threshold) of contractile markers and progerin, values that effectively removing most background noise were used. For determination of maximum values (upper display threshold) of contractile markers, the threshold was judged by evaluation of images of early-passage VSMCs, which showed relatively higher signal intensity of markers compared to late-passage cells. The ideal threshold values allowed images displaying small portion of image saturation with the clear filamentous appearance of contractile markers. Given that VSMC contractile markers were actin isoform ( $\alpha$ -SMA) or actin-associated proteins (SM22 and Calponin-1), cells with signal overlap between marker and F-actin (labelled by phalloidin) were recognized as positive-expressing cells. For the determination of maximum value of progerin, the value allowing cells of low progerin expression to be visible in images was set as the ideal upper threshold. Cells with Progerin-FLAG signals highly co-localizing with their nuclei (labelled by DAPI) were considered as positive

progerin-expressing cells.



## 2.10 RNA extraction

Total RNA was extracted using RNeasy Plus Micro kit (Qiagen) according to the manufacturer's protocol, including the optional addition of 20ng carrier RNA. RNA quality and quantity were assessed by a Nanodrop spectrophotometer at 260 nm and 280 nm ( $A_{260}/A_{280} > 1.80$ ).

## 2.11 cDNA synthesis and Quantitative Polymerase Chain Reaction (qPCR)

96ng of RNA per sample was reversely transcribed to cDNA in a 20 $\mu$ l volume reaction using SuperScript<sup>TM</sup> VILO<sup>TM</sup> Master Mix (Invitrogen). Reverse transcription was performed in three steps: 10 min at 25 °C, 10 min at 50 °C, and 5 min at 85 °C. qPCR reactions were carried out by LightCycler<sup>®</sup> 96 (Roche) with the use of 96-well plates (Roche Cat#04729692001). Reaction for each gene was performed in duplicate. Reaction in each well contained 5 $\mu$ l cDNA template (20 $\mu$ l cDNA was diluted 4x in DI water to give 80 $\mu$ l of cDNA working solution for 16 reactions), 10 $\mu$ l iQ<sup>TM</sup> SYBR<sup>®</sup> Green Supermix 2x (Bio-Rad), 1 $\mu$ l primer pair, and 4 $\mu$ l DI water. The thermal procedure initiated with pre-incubation 10min at 95 °C, and a three-step cycle of 10s at 95 °C, 60s at 65 °C, and 1s at 97 °C repeated 40 times. Followed by the amplification process, a melting curve analysis was performed to verify the specificity of the amplified products. Fold change of gene

expression levels was analyzed by the  $\Delta\Delta C_t$  method, and mRNA levels were normalized to reference gene *GAPDH*. Gene-specific primers were listed in Table 2.



## 2.12 Western blot

VSMC monolayer was scraped and lysed in ice-cold RIPA buffer (Abcam Cat#ab156034) supplemented with protease inhibitor (Roche) and phosphatase inhibitor (Roche). Collected lysate was placed on ice for 30 min and vortexed every ten minutes. The lysate was then centrifuged at 12000 rpm for 15mins at 4°C, and the supernatant was collected in new tube for use. Protein content was quantified by Bradford assay. To increase the sensitivity of Bradford assay, samples were measured at dual absorbance wavelengths (595 nm and 450 nm) for the estimation of protein concentration [76]. Equal amounts of protein (10 $\mu$ g) were separated at 100V for 90 min in a 4-15% gradient polyacrylamide gel (BIO-RAD Cat#4561083). Gels further underwent semi-dry transfer to PVDF membranes at 10V for half an hour. Membranes were blocked with 5% nonfat dried milk in TBST for one hour at room temperature. Afterwards, membranes were probed by Anti-GAPDH mouse antibody (Novus Cat#NB300-221) or Anti-FLAG rabbit antibody (Sigma Cat#F7425) overnight at 4°C followed by incubation with Goat anti-mouse IgG-HRP (Novus Cat# NBP1-73240) or Goat anti-rabbit IgG-HRP (Santa Cruz Cat#sc-2004) for an hour at room temperature. Membranes were then incubated in ECL

solution (Milipore Cat#WBLUF0500) for a minute and visualized by Bio-Rad ChemiDoc™ XRS+. Protein bands were quantified by Fiji, and were normalized to GAPDH.



### 2.13 Statistics

Statistical differences are determined by Fisher's test or Student's t-test for data with two groups. For data containing more than two groups, the analysis of variance (ANOVA) or Chi-square test was performed. Tukey Kramer test or Holm's sequential Bonferroni procedure was used for post hoc pair-wise comparisons. Sample size and p-values were shown within corresponding figures or figure legends. Results were presented as a mean  $\pm$  standard deviation. Statistical analysis was performed using GraphPad Prism or Microsoft Excel.



**Table 1. list of primary and secondary antibodies**

Primary antibody	Secondary antibody
Anti-alpha smooth muscle actin mouse antibody (1:500, Sigma Cat#A2547) & Anti-transgelin rabbit antibody (1:300, Abcam Cat#ab14106)	Alexa Fluor 488 goat anti-mouse IgG (1:500, Invitrogen Cat#A-11001) & Alexa Fluor 647 goat anti-rabbit IgG (1:300, Invitrogen Cat#A-21245)
Anti-alpha smooth muscle actin mouse antibody (1:500, Sigma Cat#A2547) & Anti-calponin-1 rabbit antibody (1:200, Abcam Cat#ab46794)	Alexa Fluor 488 goat anti-mouse IgG (1:500, Invitrogen Cat#A-11001) & Alexa Fluor 647 goat anti-rabbit IgG (1:300, Invitrogen Cat#A-21245)
Anti-FLAG rabbit antibody (1:300, Sigma Cat#F7425)	Alexa Fluor 647 goat anti-rabbit IgG (1:300, Invitrogen Cat#A-21245)

**Table 2. list of PCR primers**

Primer names	Accession no.	Forward (5' to 3')	Reverse (5' to 3')
Housekeeping gene			
<i>GAPDH</i>	NM_00128972	CTGCACCACCACCA	GGGCCATCCACAGT



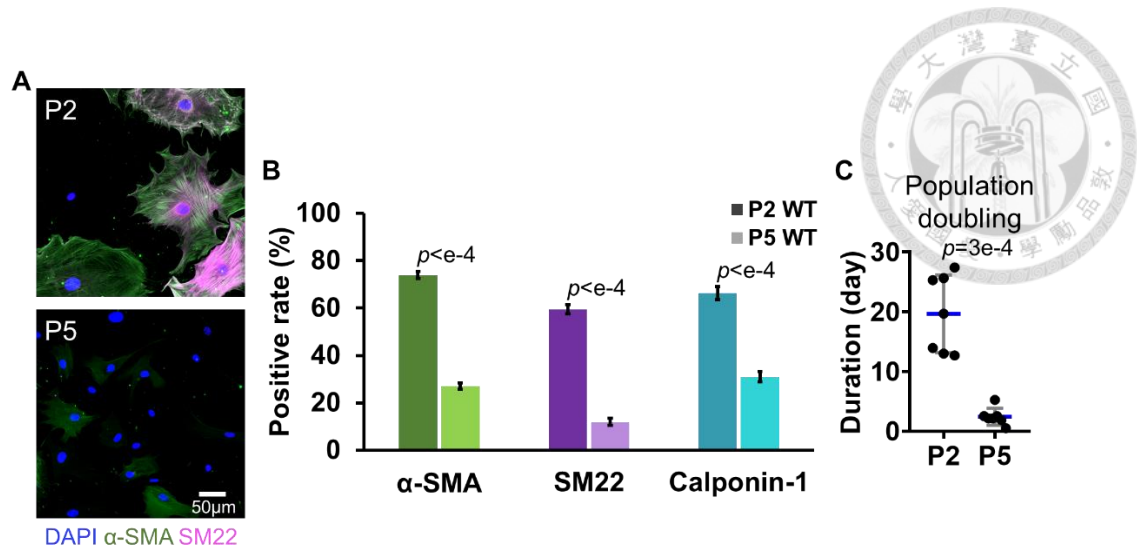
	6.1	ACTGCTTAG	CTTCT
Contractile genes			
<i>ACTA2</i>	NM_007392.3	AGAGCAAGAGAGG GATCCTGA	GTCGTCCCAGTTGG TGATGAT
<i>TAGLN</i>	NM_011526.5	TGAAGAAAGCCCAG GAGCAT	TGCTTCCCCTCCTGC AGTT
<i>MYH11</i>	NM_013607.2	GCAATGCGAAAACC GTCAA	GATGCGAATGAACT TGCCAAA
<i>CNN1</i>	XM_01124238 8.3	TCTGCACATTTTAAA CCGAGGTG	GCCAGCTTGTTCTTT ACTTCAGC
Synthetic genes			
<i>SPP1</i>	NM_00120420 1.1	AGCAAGAAACTCTT CCAAGCAA	GTGAGATTCGTCAG ATTCATCCG
<i>KLF5</i>	NM_009769.4	CGATTCACAACCCA AATTTACC	GTATGAGTCCTCAG GTGAGCTTTTA
<i>COL1A1</i>	NM_007742.4	AGAGCATGACCGAT GGATTC	AGGCCTCGGTGGAC ATTAG

## Chapter 3 Results

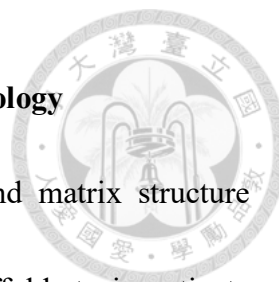


### 3.1 Establish primary VSMC culture and phenotype characterization

Compelling research had demonstrated that serial passaging promoted the phenotypic transformation of primary VSMCs, characterized by down-regulation of contractile genes and enhanced proliferation [54]. The first aim of the study was to establish primary VSMC culture and validate phenotypic changes of VSMC with serial passaging. We characterized phenotypes of P2 (early-passage) and P5 (late-passage) VSMCs by immunochemical analysis with VSMC contractile markers, including  $\alpha$ -SMA, SM22, and Calponin-1. Fluorescent images showed that great majority of P2 VSMCs expressed the contractile markers, demonstrating the establishment of primary VSMC culture. Moreover, P5 VSMCs exhibited smaller spreading area with reduced proportion of cells expressing the lineage markers compared to their P2 counterparts, indicating passage-dependent phenotypic switch (Fig 1AB). Meanwhile, P5 VSMCs had much shorter population doubling time (Fig 1C), representing phenotypic transition of VSMC as well. Taken together, we established primary VSMC culture and validated passage-dependent loss of contractile phenotype in 2D culture.

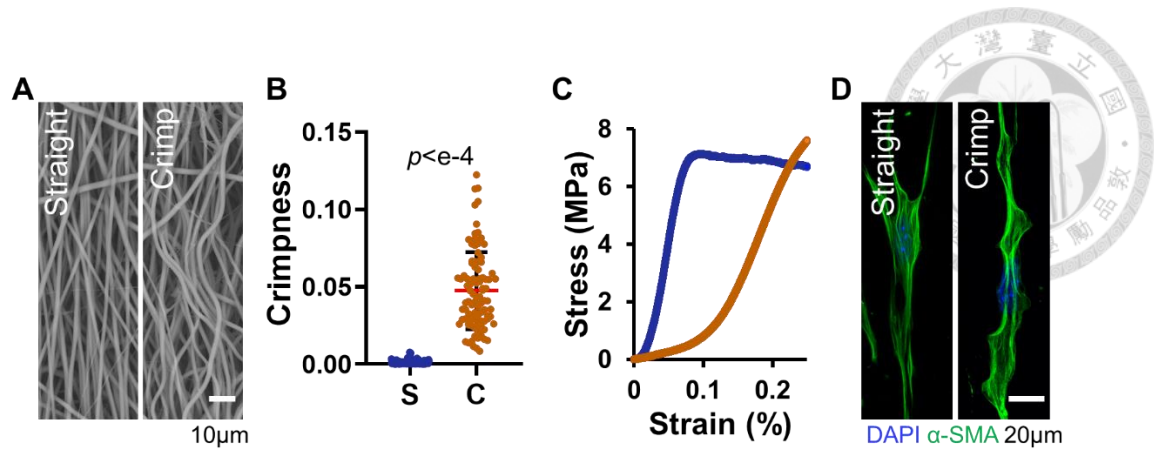


**Figure 1. Primary VSMCs exhibit passage-dependent dedifferentiation in 2D cultures.** (A) Immunofluorescence images of primary VSMCs (B) Passaging reduced proportion of cells staining positive for contractile markers ( $n > 299$ ) (C) Population doubling time reduced with subculture (P2 and P5:  $n = 7$ )

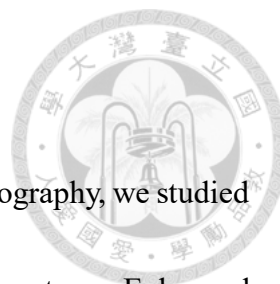


### 3.2 Characterization of biomimetic fibrous scaffolds and cell morphology

Given the correlation between VSMC phenotypic change and matrix structure during vascular pathogenesis [77], we applied electrospun 3D scaffolds to investigate structural influence of fibers on VSMC phenotype. We produced straight or wavy fibrous scaffolds to mimic the matrix architecture and mechanical behavior of disease/aged or healthy arteries (Fig 2A). Wavy scaffolds featured undulating fiber structure, and the fiber crimpness statistically differed from the straight counterpart (Fig 2B). Straight fiber structure exhibited linear mechanical behavior with higher elastic modulus while wavy structure conferred non-linear stress-strain behavior with longer toe region (Fig 2C). Straight and wavy scaffolds both provided contact guidance to modulate cell morphology (Fig 2D). In the straight scaffold, VSMC displayed elongated morphology with parallel actin filaments through the cell length. In crimp scaffold, VSMC had wavy and discontinuous actin bundles around cell periphery.

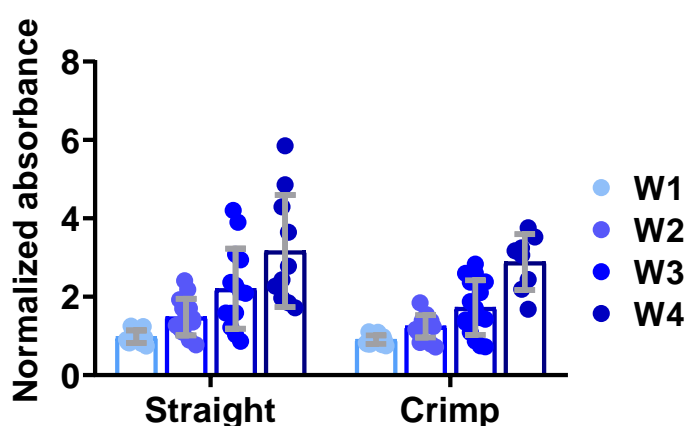


**Figure 2. Electrospun straight (S) and crimp (C) fibrous scaffolds and VSMC morphology in the scaffolds.** (A) SEM images of the fibrous scaffolds (B) Quantification of fiber structure (n=96) (C) Representative tensile stress-strain relationships of the scaffolds (D) Representative micrograph of VSMC morphology in the scaffolds.



### 3.3 Phenotypic assessment: VSMC Proliferation

Based on the morphological adaptation of VSMC in different topography, we studied the topographical regulation on P6 (late-passage) WT VSMC phenotype. Enhanced proliferation is a hallmark of VSMC dedifferentiation. We evaluated the proliferation potential of P6 VSMCs cultured in the straight and crimp scaffolds to investigate topographical influence on VSMC phenotype during the 4-week culture. By weekly monitoring cell metabolic activity with AlamarBlue assay, we indirectly accessed the growth rate of the VSMCs in the three-dimensional scaffolds. During the one-month culture period, VSMCs displayed steady growth in both scaffolds (Fig 3). Although VSMCs had the lower proliferation potential in the crimp scaffold culture, similar trends were observed in both straight and wavy scaffolds.



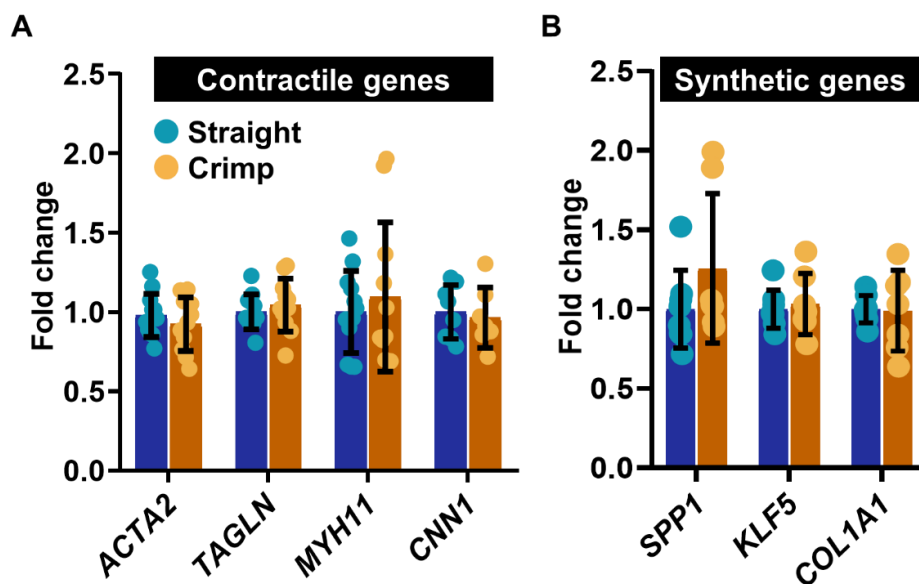
**Figure 3. Real-time monitoring of WT VSMC proliferation in fibrous scaffold.**

(Data was normalized to the day 2 baseline ; W1, W2, and W3: n=14 in the straight group, n=16 in the crimp group ; W4: n=10 in the straight group, n=8 in the crimp group)



### 3.4 Phenotypic assessment: Gene expression profile

We further examined topographical regulation of VSMC plasticity at the transcript level. Expression levels of phenotype-relevant genes were assessed by RT-qPCR. mRNA levels of contractile markers showed no differences between straight and crimp groups (Fig 4A). We also evaluated mRNA levels of synthetic markers, including matrix proteins osteopontin (gene *SPP1*), collagen type I (gene *COL1A1*), as well as the key transcriptional factor KLF5 (gene *KLF5*) (Fig 4B). PCR results suggested that there was no distinguishable effect between straight and crimp scaffolds.



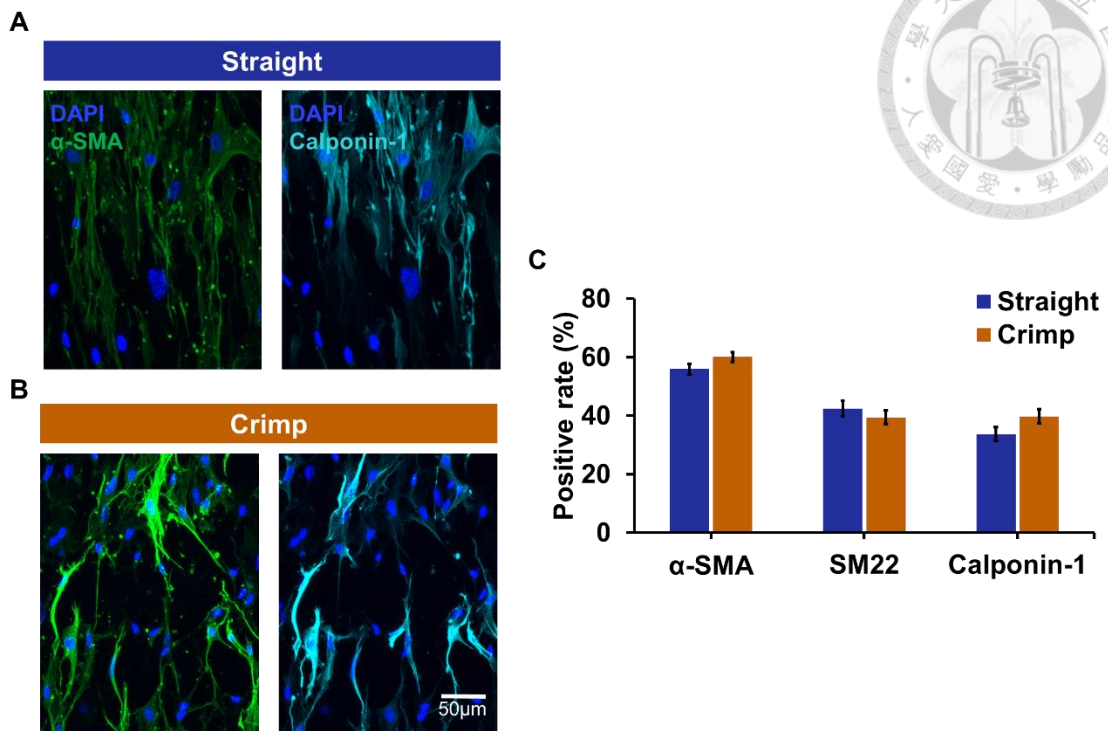
**Figure 4. Topography-dependent phenotype regulation of WT VSMC at transcript level.** (A) mRNA expression levels of contractile genes (mRNA levels of crimp group were normalized to the averages of straight counterparts, *ACTA2*, *TAGLN*, and *MYH11*: n=12 in the straight group, n=11 in crimp group ; *CNN1*: n=8 in the straight group, n=7 in the crimp group) (B) mRNA expression levels of synthetic genes (n=8 in the straight group, n=7 in the crimp group)



### 3.5 Phenotypic assessment: Immuno-characterization

We assessed contractile markers to better elucidate topographical regulation of VSMC phenotype by immunochemical analysis. Confocal images revealed that structural guidance of the scaffolds affected cell orientation. Cells in straight scaffolds formed VSMC sheet that was highly aligned, while cells in the crimp scaffolds conformed to the wavy topography with higher dispersion in cell orientation (Fig 5AB). We noticed that more VSMCs cultured in 3D scaffolds expressed contractile markers compared to 2D tissue dish culture (Fig 5C vs. 1B). However, comparison between straight and crimp scaffolds found no statistical differences (Fig 5C), suggesting weak effect of fiber structure on WT VSMC phenotype.





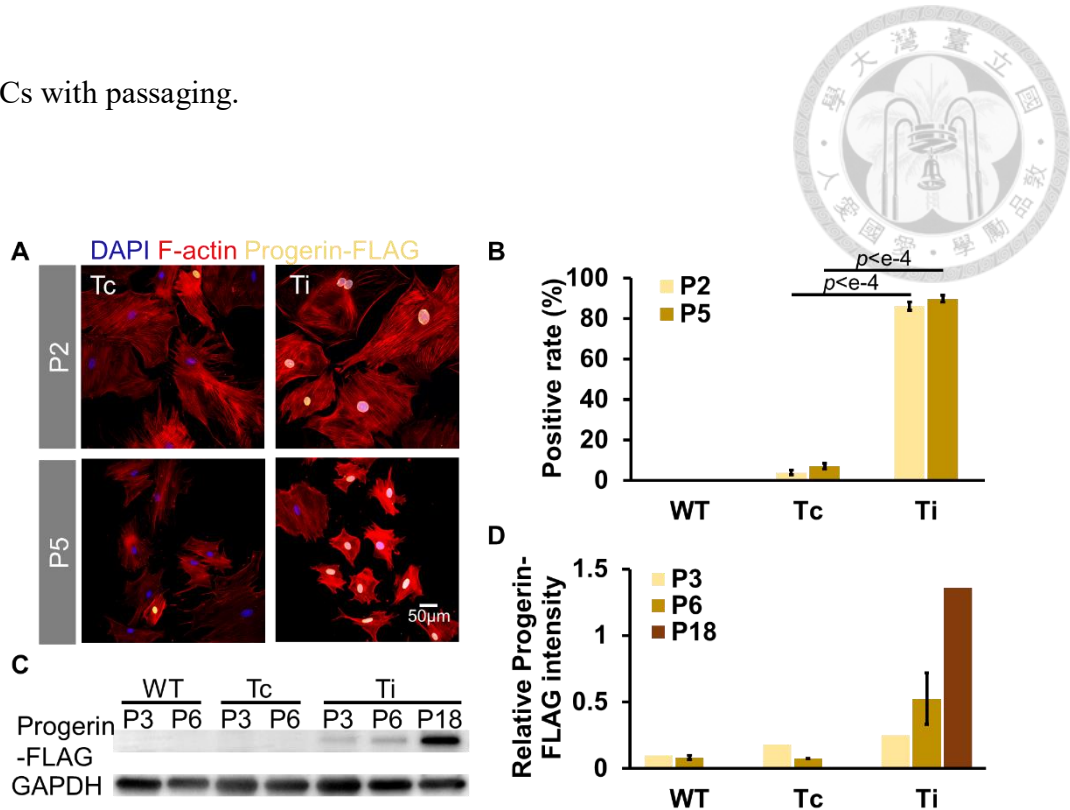
**Figure 5. Immunochemical analysis of topographical influence on VSMC phenotype.** (AB) Representative confocal images of WT VSMCs cultured in straight and crimp scaffolds (C) Quantification of marker-positive VSMCs in straight and crimp scaffolds (n>350)



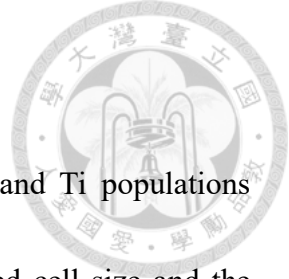
### 3.6 Progerin induction in VSMCs

Progerin expression in HGPS patients results in severe arterial remodeling, similar to geriatric cardiovascular pathology [62]. In HGPS models, VSMC is shown to be responsible for the cardiovascular dysfunction [78]. We thus investigated progerin-dependent phenotypic regulation of VSMC. Aortic VSMCs from inducible *Cre/loxP* mouse model carrying Progerin-FLAG sequence were activated by in vitro treatment of 4-Hydroxy-tamoxifen (4-OHT) at P1 to induce progerin production. VSMC without 4-OHT treatment was considered the transgenic control (Tc) against the 4-OHT induced VSMC (Ti). We validated induction efficiency by immunochemical analysis. Fluorescent images revealed that progerin was distributed around the nuclear rim (Progerin-FLAG staining in yellow, Fig 6A). Majority of P2 and P5 Ti VSMCs were progerin-positive (Fig 6AB). Low level of Cre leakage was observed in P2 and P5 Tc populations (Fig 6AB). Since studies had indicated that progerin accumulated with cell passaging [79], we examined progerin protein content in early and late-passage cells. Immunoblot revealed that progerin bands were not visible in WT and Tc populations while progerin signals enhanced in Ti populations with passaging (Fig 6C). Quantification confirmed that progerin levels of Ti populations elevated in a passage-dependent manner (Fig 6D). Taken together, 4-OHT treatment effectively induced progerin expression, which accumulated

in VSMCs with passaging.

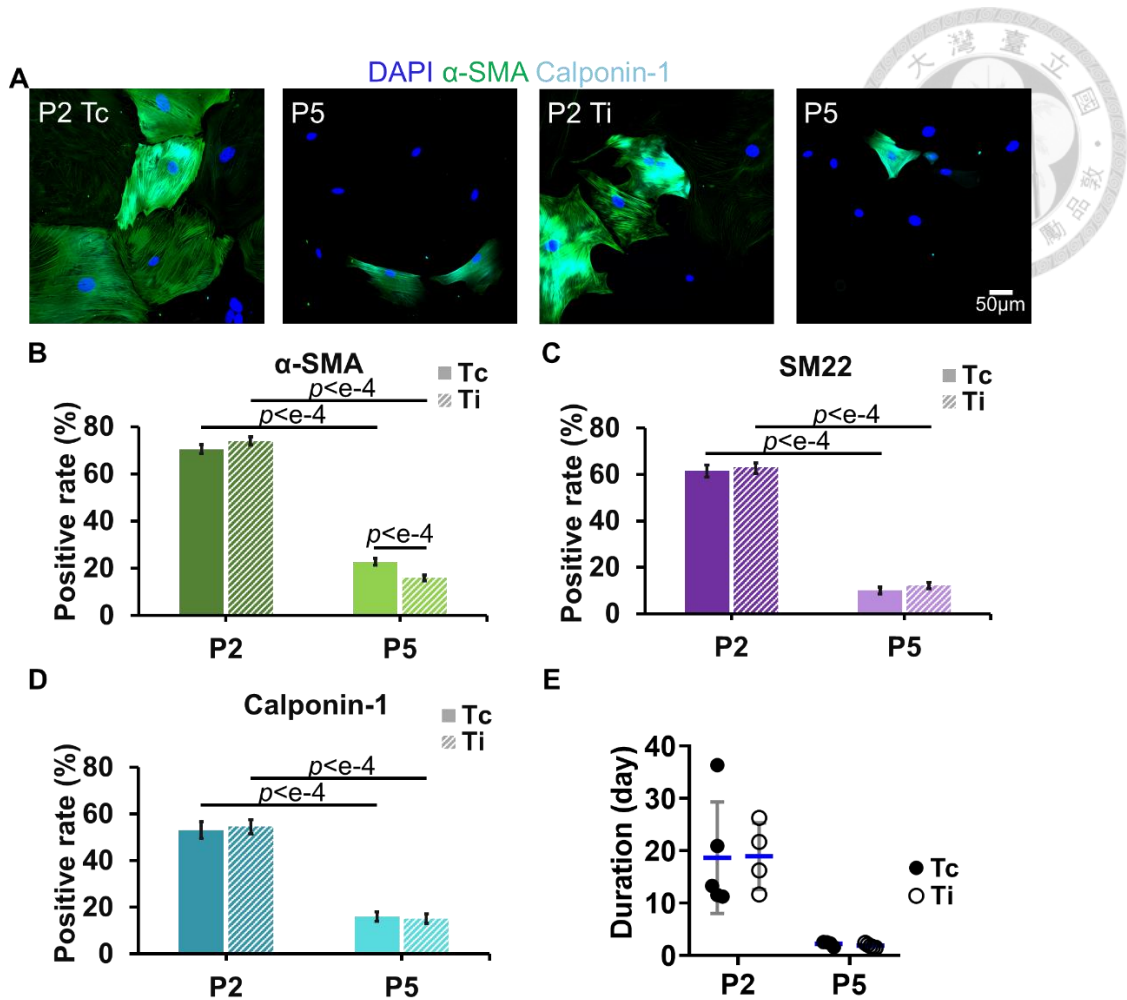


**Figure 6. In vitro treatment of 4-OHT induced progerin expression in primary VSMCs.** (A) Immunofluorescence images of progerin-expressing VSMCs (B) Percentage of progerin-positive VSMCs (n> 190) (C) Immunoblots of Progerin-FLAG (D) Protein abundance of Progerin-FLAG (normalized to the loading control GAPDH ; P6 WT, Tc, and Ti: n=2)



### 3.7 Phenotypic characterization of progerin-positive cells

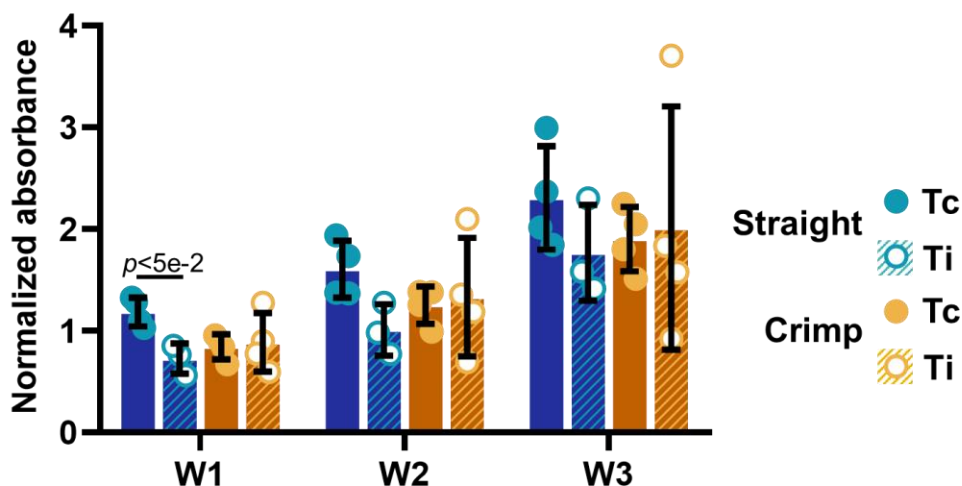
In line with the characterization results of WT VSMCs, Tc and Ti populations exhibited passage-dependent phenotypic switch, featured by reduced cell size and the expression level of contractile markers (Fig 7). P5 Ti population showed further decline in percentage of cells expressing the cytoskeleton marker  $\alpha$ -SMA compared to the P5 Tc population (Fig 7B). Moreover, Tc and Ti populations displayed decline in population doubling time with passaging, suggesting increased proliferation and changed phenotype (Fig 7E). Overall, VSMCs of Tc and Ti groups consistently displayed phenotypic switch in passage-dependent manner, but progerin had only minor effect in P5 VSMC differentiation in 2D culture.





### 3.8 Effect of progerin expression on VSMC proliferation in scaffold cultures

We performed AlamarBlue assay to examine combined effects of scaffold topography and progerin expression on P6 VSMC proliferation. Increase in metabolic activity among different groups revealed steady VSMC expansion during scaffold cultures (Fig 8). The only statistical difference was found between Tc and Ti in the straight scaffold culture in the first week. Generally, topographical cues and progerin expression did not affect the proliferation of VSMCs.

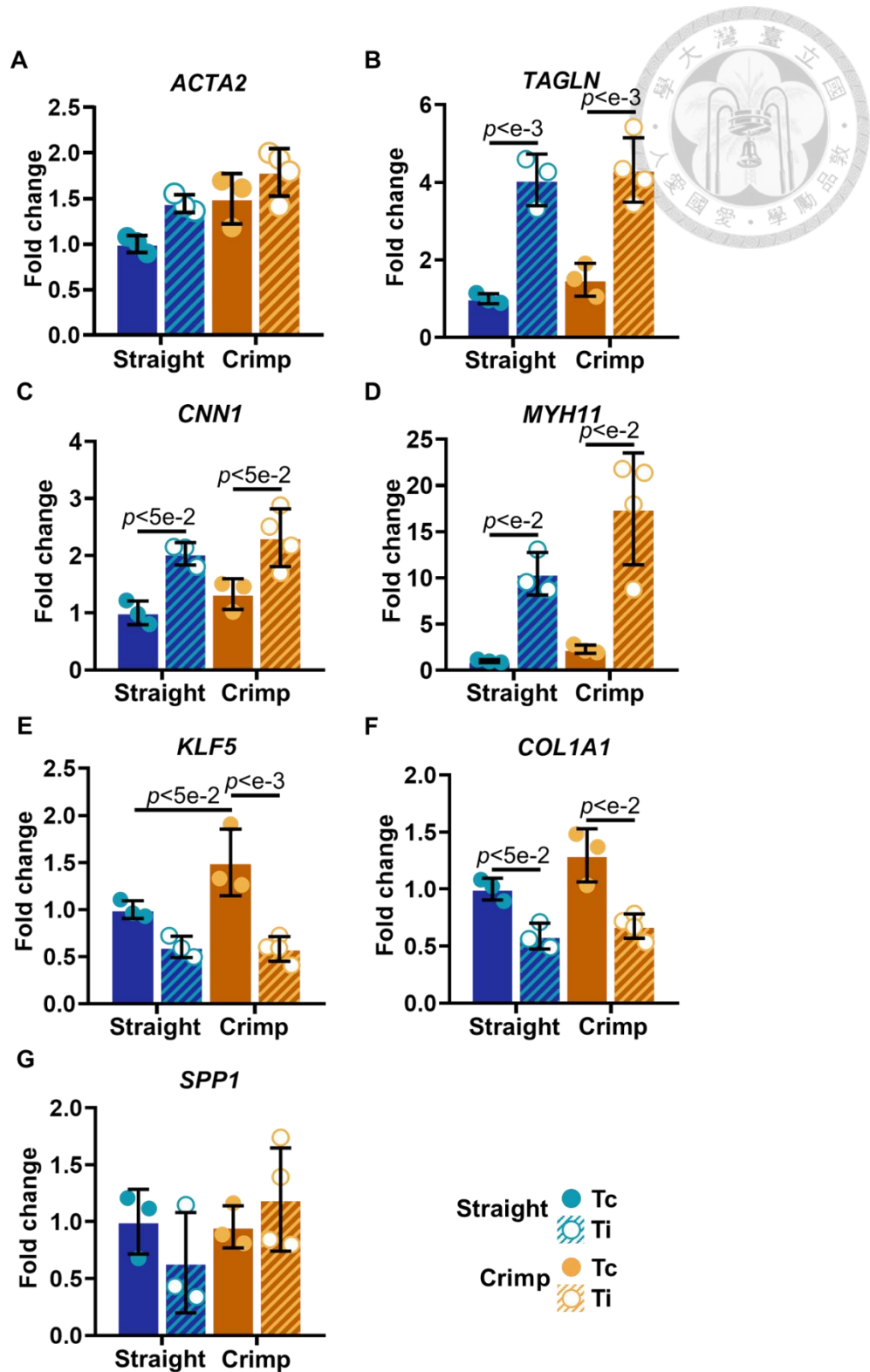


**Figure 8. Real-time proliferation monitoring of progerin-expressing VSMCs in scaffold cultures.** (Data was normalized to the day 2 baseline ; Straight TC, Ti and Crimp Ti: n=4 ; Crimp Tc: n=3)



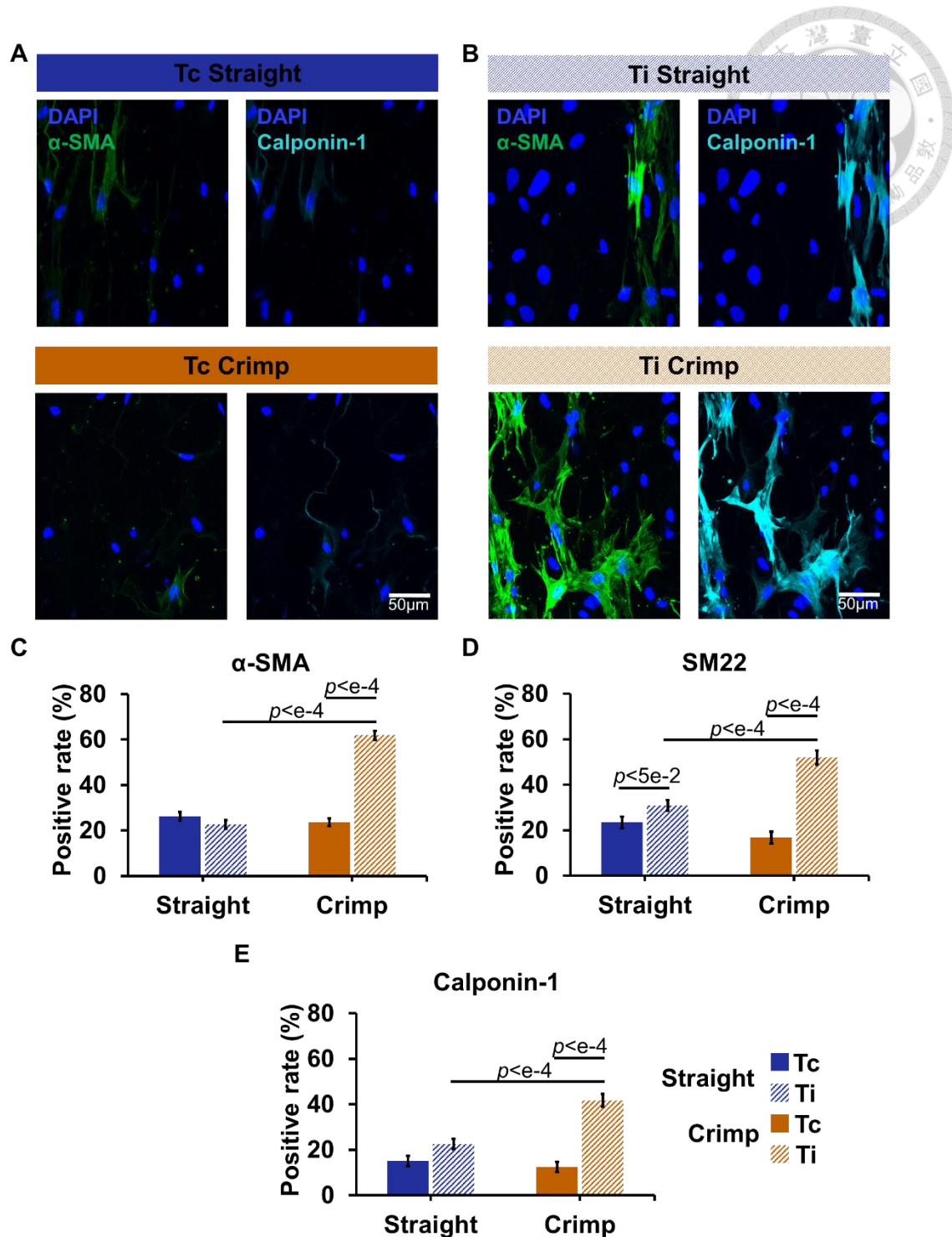
### 3.9 Effect of progerin expression on VSMC gene and protein expression in scaffold cultures

When Ti was compared to Tc within the same topographical feature, Ti populations showed consistently higher mRNA levels of all contractile genes (Fig 9). There was a small but consistent trend of further increase on the wavy scaffolds in both Tc and Ti groups. Distinct differences were also observed between Tc and Ti populations in synthetic gene profiles. Wavy scaffold culture up-regulated *KLF5* expression in Tc, but not in Ti VSMCs (Fig 9EF). We also evaluated protein levels of contractile markers by immunochemical analysis. Confocal images demonstrated elongated actin organization of Tc population in straight scaffold and curved actin arrangement in crimp scaffold (Fig 10A). Few VSMCs of Tc populations expressed contractile markers over three-week straight or crimp scaffold culture (Fig 10A). Ti population in straight scaffold exhibited spindle morphology with mild expression of contractile markers, similar to those seen in Tc group (Fig 10BDE). In the wavy scaffolds, Ti VSMCs adapted to branched actin arrangement and displayed higher levels of contractile markers (Fig 10BCDE). Combined with gene profiling and immunofluorescence results, crimp fiber structure promoted re-differentiation of progerin-expressing VSMCs.



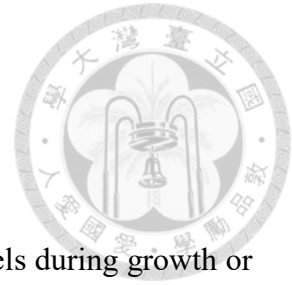
**Figure 9. Gene profiles of progerin-expressing VSMCs over three-week scaffold cultures.** (ABCD) mRNA levels of contractile genes (mRNA levels of different groups were normalized to the average of Straight Tc, Straight Tc, Ti, and Crimp Tc: n=3 ; Crimp Ti: n=4) (EFG) mRNA levels of synthetic genes





**Figure 10. Immunochemical analysis of progerin-expressing VSMCs over three-week scaffold cultures.** (A) Confocal images of Tc populations cultured in the straight or crimp scaffold (B) Confocal images of Ti populations cultured in the straight or crimp scaffold (C) Percentage of  $\alpha$ -SMA-positive cells in the straight or crimp scaffolds ( $n > 450$ ) (D) Percentage of SM22-positive cells in the straight or crimp scaffolds ( $n > 250$ ) (E) Percentage of Calponin-1-positive cells in the straight or crimp scaffolds ( $n > 220$ )

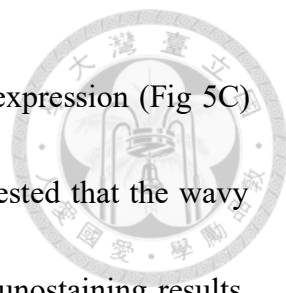
## Chapter 4 Discussion



Tunica media, the main load-bearing structure of artery, remodels during growth or aging to achieve a homeostatic stress state [80, 81]. Adverse arterial remodeling exacerbates pathogenic transformation of VSMC that further forms vicious cycle in vascular pathogenesis [58, 82]. In this study, we investigate the regulatory role of matrix architecture on VSMC.

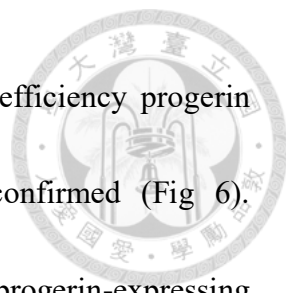
We isolated murine thoracic VSMCs and established primary culture. Due to heterogeneity of primary cell population, we used immunostaining with three differentiation markers to determine the VSMC purity at early passage number (P2). More than 60% of cells expressed differentiation markers, indicating the majority of the isolated cells were VSMCs. Passaged cells demonstrated loss expression of contractile markers, reduced cell size, and enhanced proliferation, indicating VSMC de-differentiation or phenotypic switch. While we could not exclude the contribution of cell type fluctuation to the overall phenotypic changes in late-passage population, our characterization results were consistent with findings of previous studies [54, 83].

In wild-type dedifferentiated VSMCs, straight or wavy fiber structure did not change VSMC phenotypic gene expression (Fig 4A). At the protein level and cell proliferation



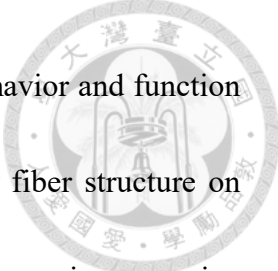
results, wavy topography had limited effects on contractile marker expression (Fig 5C) and retained VSMC in a quiescent state (Fig 3). These results suggested that the wavy topography had minimal effects on WT VSMC. According to immunostaining results, both straight and crimp 3D scaffolds largely improved VSMC contractile phenotype compared to the 2D, indicating the beneficial effect of 3D fibrous cultures (Fig 5C vs. 1B). Meanwhile, contractile marker increase in 3D scaffold cultures can be attributed to VSMC re-differentiation, indicating that majority of the cells are dedifferentiated VSMC rather than fibroblasts. Previous study in 3D had shown that VSMCs under cyclic strain exhibited better cell alignment and higher protein expression of contractile markers compared to static cultures [84]. In addition to structural mimicry, our crimp scaffolds recapitulated the non-linear mechanical behavior of healthy arteries [16, 18]. We speculate that dynamic scaffold culture would sensitize VSMC response to matrix structure and function, and may strengthen the influence of wavy topography on VSMC re-differentiation.

Since VSMC phenotypic switch, depletion, and vascular remodeling are the hallmarks of HGPS [62, 85, 86], we investigated the effect of progerin on VSMC phenotype. We established primary culture of transgenic VSMC and employed a

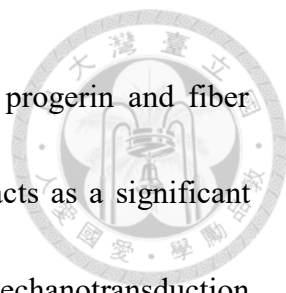


tamoxifen-inducible system to control progerin expression. High efficiency progerin induction and passage-dependent progerin accumulation were confirmed (Fig 6). Phenotypic characterization at P5 revealed decline of  $\alpha$ -SMA in progerin-expressing population compared to the transgenic control (Fig 7), indicating a mild influence of progerin on VSMC phenotype. We cultured progerin-expressing VSMCs in 3D scaffolds to examine how these cells reacted to aged/injured or healthy structures. Similar to WT cultures, progerin expression and fiber structure had no effects on VSMC proliferation (Fig 8). In transcript analysis, progerin-expressing Ti VSMCs had higher levels of contractile and lower levels of synthetic phenotype markers (Fig 9). In comparison with 2D results, progerin expression enhanced VSMC sensitivity to substrate dimensionality. Moreover, immunofluorescence revealed further enhancement of contractile markers when the progerin-expressing cells were cultured in the wavy scaffolds (Fig 10). Overall, these experiments demonstrated that progerin-expressing VSMCs are more sensitive to topographical regulation, and wavy fiber structure substantially promotes their re-differentiation. Our finding is similar to previous reports on the altered mechanotransduction of progerin-expressing cells [87-89].

VSMC plays an essential role in the development of CVDs [90], and matrix



topography is recognized as a major biophysical regulator of cell behavior and function [91]. To our knowledge, few studies emphasized the roles of wavy fiber structure on arterial function or VSMC phenotype. Our study indicated that progerin-expressing VSMCs are sensitive to fiber structure. Studies in our lab had demonstrated that wavy micro-pattern induced nuclear deformation, uneven distribution of focal adhesion, reorganization of actin structure, and increased cell tension [92, 93]. Linker of Nucleoskeleton and Cytoskeleton (LINC) complex actively remodels nucleus and nuclear lamina in response to external mechanical inputs. Abnormal expression of LINC complex member, SUN1, contributes to the nuclear defects in HGPS fibroblasts [94] As competition between inner nuclear envelope protein SUN1-microtubule coupling and SUN2-actomyosin coupling mediated homeostatic nuclear movement [95], progerin-dependent SUN1 accumulation contributed to imbalanced nucleo-cytoskeletal connections and abnormal nuclear shape [96, 97]. SUN2 and actin coupling is suggested to protect nuclear morphology under cell stretch [98], and regulates actomyosin activity and morphology of VSMCs [99]. We speculate that wavy topography regulates progerin-expressing VSMC by reinforcing SUN2-actin coupling to ameliorate nuclear defects and promote contractile phenotype. To further elucidate the structure to function link of wavy microstructure, future studies will analyze fiber waviness of aged/progeric mice aortae,

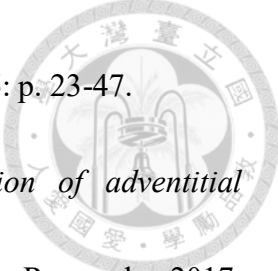


and focus on molecular pathway underlying interactions between progerin and fiber structure. In summary, our study suggests that matrix topography acts as a significant regulator of progerin-expressing VSMC, which implies that VSMC mechanotransduction is altered in disease state or in accelerated aging model. Mechanotransduction translates mechanical inputs into VSMC cytoskeletal adaptation and regulates the contractile function [100]. Our fibrous scaffolds with mechanical and structural resemblance to healthy or aged arteries offer a physiologically relevant platform for VSMC culture. Combination with mechanical stimulation will help understand how disease or aging-driven alternations such as progerin accumulation and matrix structural remodeling affect VSMC mechanosensing, and provides useful insights for the development and management of CVDs.


## References




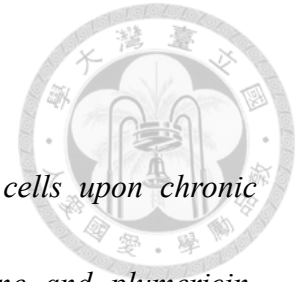
1. Wagenseil, J.E. and R.P. Mecham, *Vascular extracellular matrix and arterial mechanics*. *Physiological reviews*, 2009. **89**(3): p. 957-989.
2. Krüger-Genge, A., et al., *Vascular Endothelial Cell Biology: An Update*. *International journal of molecular sciences*, 2019. **20**(18): p. 4411.
3. Aird, W.C., *Phenotypic Heterogeneity of the Endothelium*. 2007. **100**(2): p. 158-173.
4. Nava, E. and S. Llorens, *The Local Regulation of Vascular Function: From an Inside-Outside to an Outside-Inside Model*. *Frontiers in physiology*, 2019. **10**: p. 729-729.
5. Yau, J.W., H. Teoh, and S. Verma, *Endothelial cell control of thrombosis*. *BMC Cardiovascular Disorders*, 2015. **15**(1): p. 130.
6. Mai, J., et al., *An evolving new paradigm: endothelial cells – conditional innate immune cells*. *Journal of Hematology & Oncology*, 2013. **6**(1): p. 61.
7. Majesky, M.W., et al., *The adventitia: a dynamic interface containing resident progenitor cells*. *Arteriosclerosis, thrombosis, and vascular biology*, 2011. **31**(7): p. 1530-1539.
8. Stenmark, K.R., et al., *The adventitia: essential regulator of vascular wall*

- 
- structure and function*. Annual review of physiology, 2013. **75**: p. 23-47.
9. Dutzmann, J., et al., *Sonic hedgehog-dependent activation of adventitial fibroblasts promotes neointima formation*. Cardiovascular Research, 2017. **113**(13): p. 1653-1663.
  10. Campbell, K.A., et al., *Lymphocytes and the Adventitial Immune Response in Atherosclerosis*. 2012. **110**(6): p. 889-900.
  11. Li, X.-D., et al., *Adventitial fibroblast-derived vascular endothelial growth factor promotes vasa vasorum-associated neointima formation and macrophage recruitment*. Cardiovascular Research, 2019. **116**(3): p. 708-720.
  12. Mozafari, H., C. Zhou, and L. Gu, *Mechanical contribution of vascular smooth muscle cells in the tunica media of artery*. Nanotechnology Reviews, 2019. **8**(1): p. 50-60.
  13. O'Connell, M.K., et al., *The three-dimensional micro- and nanostructure of the aortic medial lamellar unit measured using 3D confocal and electron microscopy imaging*. Matrix biology : journal of the International Society for Matrix Biology, 2008. **27**(3): p. 171-181.
  14. Cocciolone, A.J., et al., *Elastin, arterial mechanics, and cardiovascular disease*. American journal of physiology. Heart and circulatory physiology, 2018. **315**(2):

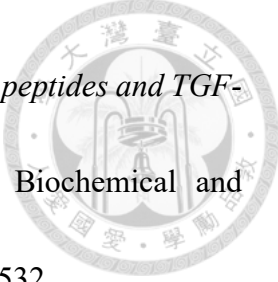


- 
- p. H189-H205.
15. Yu, X., et al., *Micromechanics of elastic lamellae: unravelling the role of structural inhomogeneity in multi-scale arterial mechanics*. 2018. **15**(147): p. 20180492.
  16. Camasão, D.B. and D. Mantovani, *The mechanical characterization of blood vessels and their substitutes in the continuous quest for physiological-relevant performances. A critical review*. *Materials Today Bio*, 2021. **10**: p. 100106.
  17. WOLINSKY, H. and S. GLAGOV, *Structural Basis for the Static Mechanical Properties of the Aortic Media*. 1964. **14**(5): p. 400-413.
  18. Shadwick, R.E., *Mechanical design in arteries*. *J Exp Biol*, 1999. **202**(Pt 23): p. 3305-13.
  19. Wen, Q. and P.A. Janmey, *Effects of non-linearity on cell-ECM interactions*. *Experimental cell research*, 2013. **319**(16): p. 2481-2489.
  20. Chistiakov, D.A., A.N. Orekhov, and Y.V. Bobryshev, *Vascular smooth muscle cell in atherosclerosis*. 2015. **214**(1): p. 33-50.
  21. Frismantiene, A., et al., *Smooth muscle cell-driven vascular diseases and molecular mechanisms of VSMC plasticity*. *Cellular Signalling*, 2018. **52**: p. 48-64.

- 
22. Rensen, S.S.M., P.A.F.M. Doevendans, and G.J.J.M. van Eys, *Regulation and characteristics of vascular smooth muscle cell phenotypic diversity*. Netherlands heart journal : monthly journal of the Netherlands Society of Cardiology and the Netherlands Heart Foundation, 2007. **15**(3): p. 100-108.
23. North, B.J. and D.A. Sinclair, *The intersection between aging and cardiovascular disease*. Circulation research, 2012. **110**(8): p. 1097-1108.
24. Yazdanyar, A. and A.B. Newman, *The burden of cardiovascular disease in the elderly: morbidity, mortality, and costs*. Clinics in geriatric medicine, 2009. **25**(4): p. 563-vii.
25. Cortes-Canteli, M. and C. Iadecola, *Alzheimer's Disease and Vascular Aging: JACC Focus Seminar*. Journal of the American College of Cardiology, 2020. **75**(8): p. 942-951.
26. El Assar, M., J. Angulo, and L. Rodríguez-Mañas, *Oxidative stress and vascular inflammation in aging*. Free Radical Biology and Medicine, 2013. **65**: p. 380-401.
27. Tousoulis, D., et al., *The role of nitric oxide on endothelial function*. Curr Vasc Pharmacol, 2012. **10**(1): p. 4-18.
28. Marín, C., et al., *Endothelial aging associated with oxidative stress can be modulated by a healthy mediterranean diet*. International journal of molecular

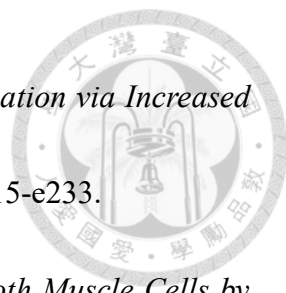



- sciences, 2013. **14**(5): p. 8869-8889.
29. Khan, S.Y., et al., *Premature senescence of endothelial cells upon chronic exposure to TNF $\alpha$  can be prevented by N-acetyl cysteine and plumericin*. Scientific reports, 2017. **7**: p. 39501-39501.
30. Izzo, C., et al., *The Role of Oxidative Stress in Cardiovascular Aging and Cardiovascular Diseases*. Life (Basel, Switzerland), 2021. **11**(1): p. 60.
31. Fhayli, W., et al., *Rise and fall of elastic fibers from development to aging. Consequences on arterial structure-function and therapeutical perspectives*. Matrix Biology, 2019. **84**: p. 41-56.
32. Chirinos, J.A., et al., *Large-Artery Stiffness in Health and Disease: JACC State-of-the-Art Review*. Journal of the American College of Cardiology, 2019. **74**(9): p. 1237-1263.
33. Greenwald, S., *Ageing of the conduit arteries*. 2007. **211**(2): p. 157-172.
34. McNulty, M., et al., *Aging is associated with increased matrix metalloproteinase-2 activity in the human aorta\**. American Journal of Hypertension, 2005. **18**(4): p. 504-509.
35. Atkinson, J., *Age-related medial elastocalcinosis in arteries: mechanisms, animal models, and physiological consequences*. 2008. **105**(5): p. 1643-1651.


- 
36. Simionescu, A., K. Philips, and N. Vyavahare, *Elastin-derived peptides and TGF- $\beta$ 1 induce osteogenic responses in smooth muscle cells*. *Biochemical and Biophysical Research Communications*, 2005. **334**(2): p. 524-532.
37. Humphrey, J.D. and G. Tellides, *Central artery stiffness and thoracic aortopathy*. *Am J Physiol Heart Circ Physiol*, 2019. **316**(1): p. H169-h182.
38. Lacolley, P., et al., *Vascular Smooth Muscle Cells and Arterial Stiffening: Relevance in Development, Aging, and Disease*. 2017. **97**(4): p. 1555-1617.
39. Nilsson, P.M., et al., *Early vascular ageing in translation: from laboratory investigations to clinical applications in cardiovascular prevention*. 2013. **31**(8): p. 1517-1526.
40. Spinetti, G., et al., *Rat Aortic MCP-1 and Its Receptor CCR2 Increase With Age and Alter Vascular Smooth Muscle Cell Function*. 2004. **24**(8): p. 1397-1402.
41. Wang, M., et al., *A Local Proinflammatory Signalling Loop Facilitates Adverse Age-Associated Arterial Remodeling*. *PLOS ONE*, 2011. **6**(2): p. e16653.
42. Chen, Y., X. Zhao, and H. Wu, *Arterial Stiffness*. 2020. **40**(5): p. 1078-1093.
43. Doran, A.C., N. Meller, and C.A. McNamara, *Role of Smooth Muscle Cells in the Initiation and Early Progression of Atherosclerosis*. 2008. **28**(5): p. 812-819.
44. Allahverdian, S., C. Ortega, and G.A. Francis, *Smooth Muscle Cell-Proteoglycan-*



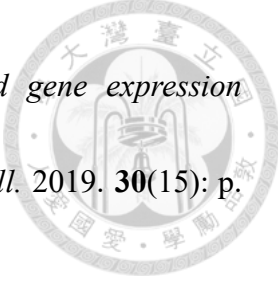
- Lipoprotein Interactions as Drivers of Atherosclerosis*. Handbook of experimental pharmacology, 2020.
45. Wang, Y., et al., *Smooth Muscle Cells Contribute the Majority of Foam Cells in ApoE (Apolipoprotein E)-Deficient Mouse Atherosclerosis*. 2019. **39**(5): p. 876-887.
  46. Yap, C., et al., *Six Shades of Vascular Smooth Muscle Cells Illuminated by KLF4 (Kruppel-Like Factor 4)*. 2021. **41**(11): p. 2693-2707.
  47. Findeisen, H.M., F.K. Kahles, and D. Bruemmer, *Epigenetic Regulation of Vascular Smooth Muscle Cell Function in Atherosclerosis*. Current Atherosclerosis Reports, 2013. **15**(5): p. 319.
  48. McDonald, O.G., et al., *Control of SRF binding to CArG box chromatin regulates smooth muscle gene expression in vivo*. The Journal of clinical investigation, 2006. **116**(1): p. 36-48.
  49. Liu, Y., et al., *Kruppel-like Factor 4 Abrogates Myocardin-induced Activation of Smooth Muscle Gene Expression\**. Journal of Biological Chemistry, 2005. **280**(10): p. 9719-9727.
  50. Liu, R., K.L. Leslie, and K.A. Martin, *Epigenetic regulation of smooth muscle cell plasticity*. Biochimica et biophysica acta, 2015. **1849**(4): p. 448-453.


- 
51. Jeong, K., et al., *FAK Activation Promotes SMC Dedifferentiation via Increased DNA Methylation in Contractile Genes*. 2021. **129**(12): p. e215-e233.
52. Harman, J.L., et al., *Epigenetic Regulation of Vascular Smooth Muscle Cells by Histone H3 Lysine 9 Dimethylation Attenuates Target Gene-Induction by Inflammatory Signaling*. 2019. **39**(11): p. 2289-2302.
53. Stegemann, J.P., H. Hong, and R.M. Nerem, *Mechanical, biochemical, and extracellular matrix effects on vascular smooth muscle cell phenotype*. 2005. **98**(6): p. 2321-2327.
54. Chang, S., et al., *Phenotypic modulation of primary vascular smooth muscle cells by short-term culture on micropatterned substrate*. PloS one, 2014. **9**(2): p. e88089-e88089.
55. Winkler, J., et al., *Concepts of extracellular matrix remodelling in tumour progression and metastasis*. Nature Communications, 2020. **11**(1): p. 5120.
56. Thyberg, J. and A. Hultgårdh-Nilsson, *Fibronectin and the basement membrane components laminin and collagen type IV influence the phenotypic properties of subcultured rat aortic smooth muscle cells differently*. Cell and Tissue Research, 1994. **276**(2): p. 263-271.
57. Sazonova, O.V., et al., *Extracellular matrix presentation modulates vascular*

- 
- smooth muscle cell mechanotransduction*. *Matrix Biology*, 2015. **41**: p. 36-43.
58. Brooke, B.S., A. Bayes-Genis, and D.Y. Li, *New Insights into Elastin and Vascular Disease*. *Trends in Cardiovascular Medicine*, 2003. **13**(5): p. 176-181.
59. Brown, X.Q., et al., *Effect of substrate stiffness and PDGF on the behavior of vascular smooth muscle cells: implications for atherosclerosis*. *Journal of cellular physiology*, 2010. **225**(1): p. 115-122.
60. Xie, S.-A., et al., *Matrix stiffness determines the phenotype of vascular smooth muscle cell in vitro and in vivo: Role of DNA methyltransferase 1*. *Biomaterials*, 2018. **155**: p. 203-216.
61. Thakar, R.G., et al., *Regulation of vascular smooth muscle cells by micropatterning*. *Biochemical and Biophysical Research Communications*, 2003. **307**(4): p. 883-890.
62. Olive, M., et al., *Cardiovascular pathology in Hutchinson-Gilford progeria: correlation with the vascular pathology of aging*. *Arteriosclerosis, thrombosis, and vascular biology*, 2010. **30**(11): p. 2301-2309.
63. Hamczyk, M.R., L. del Campo, and V. Andrés, *Aging in the Cardiovascular System: Lessons from Hutchinson-Gilford Progeria Syndrome*. *Annu Rev Physiol*, 2018. **80**: p. 27-48.

- 
64. Scaffidi, P. and T. Misteli, *Lamin A-dependent nuclear defects in human aging*. Science (New York, N.Y.), 2006. **312**(5776): p. 1059-1063.
65. Del Campo, L., et al., *Vascular Smooth Muscle Cell-Specific Progerin Expression Provokes Contractile Impairment in a Mouse Model of Hutchinson-Gilford Progeria Syndrome that Is Ameliorated by Nitrite Treatment*. Cells, 2020. **9**(3): p. 656.
66. Hamczyk, M.R. and V. Andrés, *Vascular smooth muscle cell loss underpins the accelerated atherosclerosis in Hutchinson-Gilford progeria syndrome*. Nucleus (Austin, Tex.), 2019. **10**(1): p. 28-34.
67. Dahl, K.N., et al., *Distinct structural and mechanical properties of the nuclear lamina in Hutchinson-Gilford progeria syndrome*. Proceedings of the National Academy of Sciences of the United States of America, 2006. **103**(27): p. 10271-10276.
68. Vidak, S. and R. Foisner, *Molecular insights into the premature aging disease progeria*. Histochem Cell Biol, 2016. **145**(4): p. 401-17.
69. McCord, R.P., et al., *Correlated alterations in genome organization, histone methylation, and DNA-lamin A/C interactions in Hutchinson-Gilford progeria syndrome*. Genome research, 2013. **23**(2): p. 260-269.



- 
70. Osmanagic-Myers, S. and R. Foisner, *The structural and gene expression hypotheses in laminopathic diseases—not so different after all*. 2019. **30**(15): p. 1786-1790.
71. Wang, X., B. Ding, and B. Li, *Biomimetic electrospun nanofibrous structures for tissue engineering*. *Materials Today*, 2013. **16**(6): p. 229-241.
72. Zhang, Q., et al., *Biofabrication of tissue engineering vascular systems*. 2021. **5**(2): p. 021507.
73. Jun, I., et al., *Electrospun Fibrous Scaffolds for Tissue Engineering: Viewpoints on Architecture and Fabrication*. *International journal of molecular sciences*, 2018. **19**(3): p. 745.
74. Reid, J.A., A. McDonald, and A. Callanan, *Electrospun fibre diameter and its effects on vascular smooth muscle cells*. *Journal of materials science. Materials in medicine*, 2021. **32**(10): p. 131-131.
75. Yi, B., et al., *Stiffness of Aligned Fibers Regulates the Phenotypic Expression of Vascular Smooth Muscle Cells*. *ACS Applied Materials & Interfaces*, 2019. **11**(7): p. 6867-6880.
76. Au - Ernst, O. and T. Au - Zor, *Linearization of the Bradford Protein Assay*. *JoVE*, 2010(38): p. e1918.

- 
77. van Varik, B.J., et al., *Mechanisms of arterial remodeling: lessons from genetic diseases*. *Frontiers in genetics*, 2012. **3**: p. 290-290.
78. Benedicto, I., B. Dorado, and V. Andrés, *Molecular and Cellular Mechanisms Driving Cardiovascular Disease in Hutchinson-Gilford Progeria Syndrome: Lessons Learned from Animal Models*. *Cells*, 2021. **10**(5): p. 1157.
79. Goldman, R.D., et al., *Accumulation of mutant lamin A causes progressive changes in nuclear architecture in Hutchinson–Gilford progeria syndrome*. 2004. **101**(24): p. 8963-8968.
80. Holzapfel, G.A. and R.W. Ogden, *Biomechanical relevance of the microstructure in artery walls with a focus on passive and active components*. 2018. **315**(3): p. H540-H549.
81. Morin, C., W. Krasny, and S. Avril, *Multiscale Mechanical Behavior of Large Arteries*. 2017.
82. Pai, A., et al., *Elastin degradation and vascular smooth muscle cell phenotype change precede cell loss and arterial medial calcification in a uremic mouse model of chronic kidney disease*. *The American journal of pathology*, 2011. **178**(2): p. 764-773.
83. Wang, L., et al., *Cartilage Oligomeric Matrix Protein Maintains the Contractile*



- Phenotype of Vascular Smooth Muscle Cells by Interacting With*  
*&#x3b1;*<sub>7</sub>*&#x3b2;*<sub>1</sub> *Integrin*. 2010. **106**(3): p. 514-  
525.
84. Bono, N., et al., *Unraveling the role of mechanical stimulation on smooth muscle cells: A comparative study between 2D and 3D models*. 2016. **113**(10): p. 2254-2263.
85. Varga, R., et al., *Progressive vascular smooth muscle cell defects in a mouse model of Hutchinson–Gilford progeria syndrome*. 2006. **103**(9): p. 3250-3255.
86. Coll-Bonfill, N., et al., *Progerin triggers a phenotypic switch in vascular smooth muscle cells that causes replication stress and an aging-associated secretory signature*. bioRxiv, 2022: p. 2022.02.05.479232.
87. Verstraeten, V.L.R.M., et al., *Increased mechanosensitivity and nuclear stiffness in Hutchinson-Gilford progeria cells: effects of farnesyltransferase inhibitors*. *Aging cell*, 2008. **7**(3): p. 383-393.
88. Danielsson, B.E., et al., *Lamin microaggregates lead to altered mechanotransmission in progerin-expressing cells*. *Nucleus*, 2020. **11**(1): p. 194-204.
89. Pitrez, P.R., et al., *Vulnerability of progeroid smooth muscle cells to*



- biomechanical forces is mediated by MMP13*. Nature Communications, 2020. **11**(1): p. 4110.
90. Zhuge, Y., et al., *Role of smooth muscle cells in Cardiovascular Disease*. International journal of biological sciences, 2020. **16**(14): p. 2741-2751.
91. Leclech, C. and C. Villard, *Cellular and Subcellular Contact Guidance on Microfabricated Substrates*. 2020. **8**.
92. Huang, C.-H.J., *Effect of Crimp Morphology on Cell Traction Force*. 2019.
93. Huang, B.-L., *Wavy Morphology Regulates Actin Structure and Phenotype in Vascular Smooth Muscle Cells*. 2020.
94. Chen, C.-Y., et al., *Accumulation of the inner nuclear envelope protein Sun1 is pathogenic in progeric and dystrophic laminopathies*. Cell, 2012. **149**(3): p. 565-577.
95. Zhu, R., S. Antoku, and G.G. Gundersen, *Centrifugal Displacement of Nuclei Reveals Multiple LINC Complex Mechanisms for Homeostatic Nuclear Positioning*. Current biology : CB, 2017. **27**(20): p. 3097-3110.e5.
96. Chang, W., et al., *Imbalanced nucleocytoskeletal connections create common polarity defects in progeria and physiological aging*. 2019. **116**(9): p. 3578-3583.
97. Chen, Z.-J., et al., *Dysregulated interactions between lamin A and SUN1 induce*



- abnormalities in the nuclear envelope and endoplasmic reticulum in progeric laminopathies*. *Journal of Cell Science*, 2014. **127**(8): p. 1792-1804.
98. Hoffman, L.M., et al., *Mechanical stress triggers nuclear remodeling and the formation of transmembrane actin nuclear lines with associated nuclear pore complexes*. *Mol Biol Cell*, 2020. **31**(16): p. 1774-1787.
99. Porter, L., et al., *SUN1/2 Are Essential for RhoA/ROCK-Regulated Actomyosin Activity in Isolated Vascular Smooth Muscle Cells*. 2020. **9**(1): p. 132.
100. Ye, G.J.C., A.P. Nesmith, and K.K. Parker, *The role of mechanotransduction on vascular smooth muscle myocytes' [corrected] cytoskeleton and contractile function*. *Anatomical record (Hoboken, N.J. : 2007)*, 2014. **297**(9): p. 1758-1769.